Title
Rayleigh and Wood anomalies in the diffraction of light from a perfectly conducting reflection grating

Journal
Journal of Optics (United Kingdom), 18(2)

ISSN
2040-8978

Authors
Maradudin, AA
Simonsen, I
Polanco, J
et al.

Publication Date
2016-01-06

DOI
10.1088/2040-8978/18/2/024004

IOP Publishing Journal of Optics
J. Opt. 18 (2016) 024004 (10pp) doi:10.1088/2040-8978/18/2/024004

Rayleigh and Wood anomalies in the diffraction of light from a perfectly conducting reflection grating

A A Maradudin[1,6], I Simonsen[2], J Polanco[3,4] and R M Fitzgerald[5]

[1] Department of Physics and Astronomy, University of California, Irvine, CA 92697, USA
[2] Department of Physics, Norwegian University of Science and Technology, NO-7492 Trondheim, Norway
[3] Program in Computer Sciences, University of Texas, El Paso, TX 79968, USA
[4] Department of Physics and Mathematics, Autonomous University of Ciudad Juárez, Cd. Juárez, 32310, México
[5] Department of Physics, University of Texas, El Paso, TX 79968, USA

E-mail: aamaradu@uci.edu

Received 27 October 2015, revised 1 December 2015
Accepted for publication 4 December 2015
Published 6 January 2016

Abstract

By means of a modal method we have calculated the angular dependence of the reflectivity and the efficiencies of several other diffracted orders of a perfectly conducting lamellar reflection grating illuminated by p-polarized light. These dependencies display the signatures of Rayleigh and Wood anomalies, usually associated with diffraction from a metallic grating. The Wood anomalies here are caused by the excitation of the surface electromagnetic waves supported by a periodically corrugated perfectly conducting surface, whose dispersion curves in both the nonradiative and radiative regions of the frequency-wavenumber plane are calculated.

Keywords: Rayleigh and Wood anomalies, diffraction grating, electromagnetic scattering

(Some figures may appear in colour only in the online journal)

1. Introduction

In his measurements of the angular and wavelength dependencies of light diffracted from various metallic gratings, Wood [1, 2] noted 'anomalies' in the data he obtained when the wave vector of the incident beam was in the plane perpendicular to their grooves, and its magnetic vector was parallel to the grooves, i.e. in p polarization. These anomalies were of two types.

The first type of anomaly was a discontinuous change in the reflectivity as a function of the wavelength of the incident light for a fixed angle of incidence at well-defined wavelengths. These wavelengths were independent of the metal on which the grating was ruled, and were determined by the period of the grating. It was shown by Lord Rayleigh [3, 4] that these anomalies occur at the wavelengths at which a diffracted order appears or disappears at a grazing angle. For the nth diffracted order this occurs at the wavelength given by $\lambda_n = d(\pm 1 - \sin\theta_0)/n$, where d is the period of the grating, θ_0 is the angle of incidence, and n is an integer. In the former case the power in that order is removed from the zero order beam; in the latter case the power in that order is returned to the zero-order beam.

In subsequent investigations [5, 6] it was found that such anomalies also occur at the Rayleigh wavelengths when the electric vector of the incident light is parallel to the grooves of the grating, i.e. in s polarization. However, in this case they are weak and require deep grooves for their observation.

The second type of anomaly, now called a Wood anomaly, was diffuse, and extended in a wide range of wavelengths from a Rayleigh anomaly towards longer wavelengths. These anomalies generally consisted of a maximum and minimum intensity. When the plane of incidence was perpendicular to the grooves of the grating they occurred only in p polarization, and the wavelengths at which they occurred changed when the metal on which the grating was

[6] Author to whom any correspondence should be addressed.

fabricated was changed. Wood had no explanation for these anomalies, nor did Lord Rayleigh. The explanation for them was provided many years later by Fano [7], who showed that they are due to the excitation by the incident light of the surface plasmon polaritons supported by a periodically corrugated vacuum-metal interface [8, 9]. If the dielectric function of the metal is denoted by $\epsilon(\omega)$, the wavenumber of the surface plasmon polariton, $k_{sp}(\omega) = (\omega/c)[\epsilon(\omega)/(\epsilon(\omega)+1)]^{\frac{1}{2}}$, is slightly larger than ω/c in the frequency range where $\epsilon(\omega)$ is negative. The component of the wave vector of the incident light parallel to the surface, $k = (\omega/c)\sin\theta_0$, is smaller than (ω/c). In order that momentum be conserved in the interaction of the incident wave with the surface plasmon polariton the difference between these two wave numbers has to be made up, which in the present case is done by a wave number of the grating, $2\pi n/d$, where n is an integer. The condition for the excitation of the surface plasmon polariton therefore is $k = k_{sp}(\omega) + (2\pi/d)n$, or $(1/\lambda) = (1/\lambda_{sp}(\omega)) + n/d$. Since surface plasmon polaritons propagating normal to the grooves of a metallic grating exist only in p polarization, they cannot be excited by s-polarized light when its electric vector is parallel to the grooves. Thus, Wood's anomalies do not exist in s polarization. Since the wavelength of a surface plasmon polariton is a function of the dielectric function of the metal, the scattering angles or wavelengths at which these anomalies occur vary from metal to metal.

In the years following Fano's work these grating anomalies were studied extensively by experimentalists and theorists. A recent review of developments in this field is presented in the chapter by Maystre [10].

The great majority of the theoretical studies of grating anomalies were carried out for diffraction from metallic gratings. However, there were exceptions to such studies. It had been believed that when the wavelength of the incident field was in the visible and near-infrared regions of the electromagnetic spectrum, the grating could be regarded as a perfect conductor, which led to rigorous calculations of the diffraction of light from perfectly conducting gratings [11–15]. In a particularly detailed set of calculations [15], Rayleigh anomalies were observed to occur in the wavelength dependence of the reflectivity and other diffraction efficiencies at the values predicted by Lord Rayleigh. In addition, other features were observed in these dependencies. These were referred to as resonance anomalies, and were attributed to resonances within the grooves of the grating [16]. These standing waves within the grating grooves were taken into account in reference [16] by replacing the grating by a planar surface with a periodic surface impedance (reactance). Such a structure can support leaky (complex) surface waves that produce features in the angular or wavelength dependencies of the scattering efficiencies distinct from the Rayleigh anomalies. Unfortunately, the dispersion curves of these leaky surface waves were not calculated in either reference [15] or reference [16]. Therefore, it was not possible to relate directly the existence of these waves to the Wood anomalies in the scattering efficiencies.

When results calculated on the basis of the assumption of a perfectly conducting grating were compared to experimental data for the diffraction of p-polarized light from metallic gratings in the visible and near-infrared, serious discrepancies were found [17, 18]. Interest in the diffraction of light from perfectly conducting gratings waned in the wake of these results.

Nevertheless, in this paper we revisit the theory of the diffraction of p-polarized light from a perfectly conducting grating. Our motivation for doing so is that the theoretical studies of the diffraction of p-polarized light from metallic gratings following the work of Fano recognized the origin of the Wood anomalies as the surface plasmon polaritons supported by the periodically corrugated metal surface. At the time the theoretical studies of the diffraction of p-polarized light from perfectly conducting gratings were carried out, it was not known, as it is now, that a periodically corrugated perfectly conducting surface also supports surface electromagnetic waves [19, 20].

Perhaps for this reason the dispersion curves of the surface waves supported by such surfaces, even those predicted with heuristic impedance boundary conditions, were not calculated. Now that the existence of p-polarized surface electromagnetic waves on periodically corrugated perfectly conducting surfaces is known, it seemed of interest to calculate their dispersion curves together with the angular dependencies of the diffraction efficiencies in the diffraction of p-polarized light from such gratings. The goal of these calculations is a demonstration that these surface electromagnetic waves give rise to Wood anomalies in the same way that surface plasmon polaritons give rise to Wood anomalies in the diffraction of p-polarized light from metallic gratings. It is such calculations that we carry out in this paper. In doing so we will use a modal approach analogous to the one employed by Lopez-Rios *et al* [21] to study the reflectivity of a lamellar metallic grating (see also [22] and [23]).

2. The diffracted field

The physical system we study in this work, a perfectly conducting lamellar grating, is depicted in figure 1. It is illuminated from the vacuum by a p-polarized electromagnetic field of frequency ω, whose plane of incidence, and hence of scattering, is the x_1x_3 plane. In p polarization it is convenient to work with the single nonzero component of the magnetic field, $H_2(x_1, x_3; t) = H_2(x_1, x_3|\omega)\exp(-i\omega t)$. Because of the periodicity of the surface profile, this field amplitude $H_2(x_1, x_3|\omega)$ must satisfy the Floquet–Bloch condition [24] $H_2(x_1 + d, x_3|\omega) = \exp(ikd)\, H_2(x_1, x_3|\omega)$, where $k = (\omega/c)\sin\theta_0$ is the projection of the wave vector of the incident field on the plane $x_3 = 0$, and d is the period of the grating. The angle θ_0 is the angle of incidence, measured counterclockwise from the positive x_3-axis. As a consequence the field at any point of space above the grating surface can be determined from the field in the central cell located between $x_1 = -a/2$ and $x_1 = a/2$.

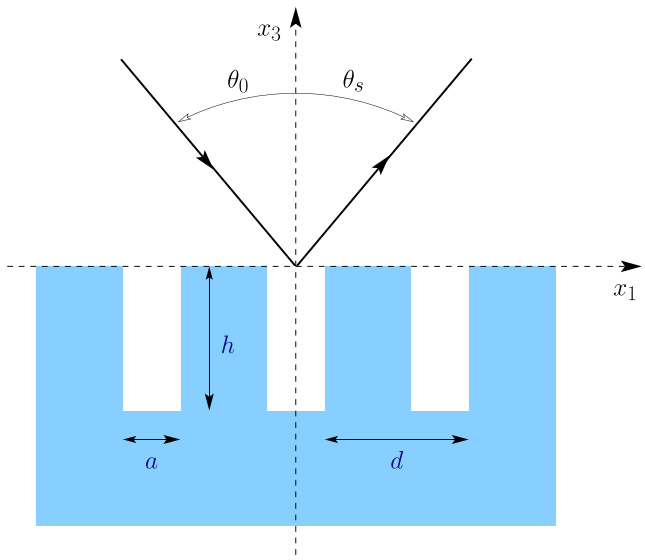

Figure 1. A depiction of the grating considered in this work, the parameters that define it, and the geometry of the diffraction of light from it.

The magnetic field in the vacuum region $x_3 > 0$ can be written

$$H_2^{>}(x_1, x_3|\omega) = \mathrm{e}^{\mathrm{i}kx_1 - \mathrm{i}\alpha_0(k)x_3} + \sum_{n=-\infty}^{\infty} A_n \mathrm{e}^{\mathrm{i}k_n x_1 + \mathrm{i}\alpha_0(k_n)x_3}, \quad (1)$$

where $k_n = k + 2\pi n/d$, and

$$\alpha_0(k) = \left[\left(\frac{\omega}{c}\right)^2 - k^2\right]^{1/2}. \quad (2)$$

The manner in which the branch cut defining the square root in equation (2) is obtained, will be explained below.

The magnetic field within the central groove of the grating, defined by $-a/2 < x_1 < a/2$, $-h < x_3 < 0$, that satisfies the boundary conditions [25]

$$\frac{\partial}{\partial x_1} H_2^{<}(\pm a/2, x_3|\omega) = 0, \ -h < x_3 < 0, \quad (3a)$$

$$\frac{\partial}{\partial x_3} H_2^{<}(x_1, -h|\omega) = 0, \ -a/2 < x_1 < a/2, \quad (3b)$$

can be written

$$H_2^{<}(x_1, x_3|\omega) = \sum_{m=0}^{\infty} B_m \cos\left[\frac{m\pi}{a}\left(x_1 - \frac{a}{2}\right)\right] \times \cos\left[\alpha_m(\omega)(x_3 + h)\right], \quad (4)$$

where

$$\alpha_m(\omega) = \left[\left(\frac{\omega}{c}\right)^2 - \left(\frac{m\pi}{a}\right)^2\right]^{\frac{1}{2}} \quad \mathrm{R}\alpha_m(\omega) > 0, \ \mathrm{I}\alpha_m(\omega) > 0. \quad (5)$$

The amplitudes $\{A_n\}$ and $\{B_n\}$ are obtained from the remaining boundary conditions satisfied by the magnetic field, namely [25]

$$\frac{\partial}{\partial x_3} H_2^{>}(x_1, 0|\omega) = 0, \quad a/2 < |x_1| < d/2, \quad (6a)$$

$$\frac{\partial}{\partial x_3} H_2^{>}(x_1, 0|\omega) = \frac{\partial}{\partial x_3} H_2^{<}(x_1, 0|\omega), \ -a/2 < x_1 < a/2, \quad (6b)$$

$$H_2^{>}(x_1, 0|\omega) = H_2^{<}(x_1, 0|\omega), \ -a/2 < x_1 < a/2. \quad (6c)$$

We first consider equation (6*b*) which, with equations (1) and (4), becomes (for $-a/2 < x_1 < a/2$)

$$-\mathrm{i}\alpha_0(k)\mathrm{e}^{\mathrm{i}kx_1} + \sum_{n=-\infty}^{\infty} \mathrm{i}\alpha_0(k_n)A_n \mathrm{e}^{\mathrm{i}k_n x_1} = -\sum_{m=0}^{\infty} \alpha_m(\omega)B_m \cos\left[\frac{m\pi}{a}\left(x_1 - \frac{a}{2}\right)\right] \sin\left[\alpha_m(\omega)h\right]. \quad (7)$$

We next multiply this equation by $\exp(-\mathrm{i}k_j x_1)$ and integrate the result with respect to x_1 over the period d:

$$-\mathrm{i}\alpha_0(k)\int_{-\frac{d}{2}}^{\frac{d}{2}} \mathrm{d}x_1 \mathrm{e}^{\mathrm{i}(k-k_j)x_1} + \sum_{n=-\infty}^{\infty} \mathrm{i}\alpha_0(k_n)A_n \int_{-\frac{d}{2}}^{\frac{d}{2}} \mathrm{d}x_1 \mathrm{e}^{\mathrm{i}(k_n-k_j)x_1} = -\sum_{m=0}^{\infty} \alpha_m(\omega)B_m \sin\left[\alpha_m(\omega)h\right] \times \int_{-\frac{a}{2}}^{\frac{a}{2}} \mathrm{d}x_1 \mathrm{e}^{-\mathrm{i}k_j x_1} \cos\left[\frac{m\pi}{a}\left(x_1 - \frac{a}{2}\right)\right]. \quad (8)$$

It should be kept in mind that according to equation (6*a*) the function represented by the coefficient of $\exp(-\mathrm{i}k_j x_1)$ in the integrand on the left-hand side of this equation vanishes for $a/2 < |x_1| < d/2$.

Equation (8) can be rewritten as

$$-\mathrm{i}\alpha_0(k)\mathrm{d}\delta_{j0} + \mathrm{i}\alpha_0(k_j)\mathrm{d}A_j = -\sum_{m=0}^{\infty} S_{jm}\alpha_m(\omega)aB_m \sin\left[\alpha_m(\omega)h\right], \quad (9)$$

where

$$S_{jm} = \frac{1}{a}\int_{-\frac{a}{2}}^{\frac{a}{2}} \mathrm{d}x_1 \mathrm{e}^{-\mathrm{i}k_j x_1} \cos\left[\frac{m\pi}{a}\left(x_1 - \frac{a}{2}\right)\right], = \frac{\exp(-\mathrm{i}m\pi/2)}{2}\mathrm{sinc}\left(\frac{k_j a}{2} - \frac{m\pi}{2}\right) + \frac{\exp(\mathrm{i}m\pi/2)}{2}\mathrm{sinc}\left(\frac{k_j a}{2} + \frac{m\pi}{2}\right), \quad (10)$$

with $\mathrm{sinc}(x) = \sin(x)/x$.

Thus, the first relation between the $\{A_n\}$ and $\{B_m\}$ becomes

$$A_j = \delta_{j0} + \mathrm{i}\frac{a}{d}\frac{1}{\alpha_0(k_j)}\sum_{m=0}^{\infty} S_{jm}\alpha_m(\omega)\sin\left[\alpha_m(\omega)h\right]B_m. \quad (11)$$

A second relation between the $\{A_n\}$ and $\{B_m\}$ is obtained by starting with the boundary condition (6*c*). With the use of equations (1) and (4) it becomes

$$\mathrm{e}^{\mathrm{i}k x_1} + \sum_{n=-\infty}^{\infty} A_n \mathrm{e}^{\mathrm{i}k_n x_1} = \sum_{m=0}^{\infty} B_m \cos\left[\frac{m\pi}{a}\left(x_1 - \frac{a}{2}\right)\right] \times \cos\left[\alpha_m(\omega)h\right], \quad -\frac{a}{2} < x_1 < \frac{a}{2}. \quad (12)$$

We multiply this equation by $\cos\left[\frac{j\pi}{a}(x_1 - \frac{a}{2})\right]$ and integrate the result with respect to x_1 over the interval $(-a/2, a/2)$. In this way we obtain the equation

$$\int_{-\frac{a}{2}}^{-\frac{a}{2}} \mathrm{d}x_1 \cos\left[\frac{j\pi}{a}\left(x_1 - \frac{a}{2}\right)\right]\mathrm{e}^{\mathrm{i}kx_1} + \sum_{n=-\infty}^{\infty} A_n \int_{-\frac{a}{2}}^{\frac{a}{2}} \mathrm{d}x_1 \cos\left[\frac{j\pi}{a}\left(x_1 - \frac{a}{2}\right)\right]\mathrm{e}^{\mathrm{i}k_n x_1} = \sum_{m=0}^{\infty} B_m \cos\left[\alpha_m(\omega)h\right] \int_{-\frac{a}{2}}^{\frac{a}{2}} \mathrm{d}x_1 \cos\left[\frac{j\pi}{a}\left(x_1 - \frac{a}{2}\right)\right] \times \cos\left[\frac{m\pi}{a}\left(x_1 - \frac{a}{2}\right)\right]. \quad (13)$$

With the aid of equation (10) this equation becomes

$$aS_{0j}^{*} + a\sum_{n=-\infty}^{\infty} A_n S_{nj}^{*} = \frac{a}{2\epsilon_j}\cos\left[\alpha_j(\omega)h\right]B_j, \quad (14)$$

where

$$\epsilon_j = \begin{cases} 1/2, & j = 0, \\ 1, & j \geqslant 1. \end{cases} \quad (15)$$

It follows from equation (14) that

$$B_j = \frac{2\epsilon_j}{\cos\left[\alpha_j(\omega)h\right]}\left[S_{0j}^{*} + \sum_{n=-\infty}^{\infty} A_n S_{nj}^{*}\right]. \quad (16)$$

On combining equations (11) and (16) we obtain the equation satisfied by the $\{A_n\}$:

$$A_m = \delta_{m0} + M_{m0}(k, \omega) + \sum_{n=-\infty}^{\infty} M_{mn}(k, \omega)A_n, \quad m = 0, \pm 1, \pm 2, \ldots, \quad (17)$$

where

$$M_{mn}(k, \omega) = 2\mathrm{i}\frac{a}{d}\frac{1}{\alpha_0(k_m)}\sum_{r=0}^{\infty}\epsilon_r S_{mr}S_{nr}^{*}\alpha_r(\omega)\tan\left[\alpha_r(\omega)h\right]. \quad (18)$$

The diffraction efficiency of the mth diffracted beam is given by

$$e_m = \frac{\alpha_0(k_m)}{\alpha_0(k)}|A_m|^2. \quad (19)$$

The conservation of energy in the diffraction process is expressed by

$$\sum_{m}{}' \frac{\alpha_0(k_m)}{\alpha_0(k)}|A_m|^2 = 1, \quad (20)$$

where the prime on the sum denotes that it extends over only the open channels, i.e. the ones for which $\alpha_0(k_m)$ is real. Finally, the reflectivity is given by

$$R = e_0 = |A_0|^2. \quad (21)$$

3. The dispersion relation for surface electromagnetic waves

To obtain the dispersion relation for the surface electromagnetic waves supported by the perfectly conducting lamellar grating depicted in figure 1, we need only to omit the incident field from the right hand side of equation (1). This is equivalent to deleting the inhomogeneous terms from equation (17). In this way we obtain the homogeneous system of equations

$$A_m = \sum_{n=-\infty}^{\infty} M_{mn}(k, \omega)A_n, \qquad m = 0, \pm 1, \pm 2, \ldots. \quad (22)$$

The solvability condition for this system of equations

$$\det\left[M_{mn}(k, \omega) - \delta_{mn}\right] = 0, \quad (23)$$

is the dispersion relation we seek.

The magnetic field of the surface wave is then given by the second term on the right hand side of equation (1)

$$H_2^{>}(x_1, x_3|\omega) = \sum_{n=-\infty}^{\infty} A_n \mathrm{e}^{\mathrm{i}k_n x_1 + \mathrm{i}\alpha_0(k_n)x_3}. \quad (24)$$

At the same time, to avoid working with a matrix that is singular when $\alpha_0(k_m)$ vanishes, we rewrite equation (23) as

$$D(k, \omega) = \det\left[N_{mn}(k, \omega) + \mathrm{i}h\alpha_0(k_m)\delta_{mn}\right] = 0, \quad (25)$$

where

$$N_{mn}(k, \omega) = 2\frac{a}{d}\sum_{r=0}^{\infty}\epsilon_r S_{mr}S_{nr}^{*}\alpha_r(\omega)h\tan\left[\alpha_r(\omega)h\right]. \quad (26)$$

The solutions $\omega(k)$ of equation (25) are even functions of k, $\omega(-k) = \omega(k)$. They are also periodic functions of k with period $2\pi/d$, $\omega(k + 2\pi/d) = \omega(k)$. Thus, in the reduced zone scheme we need to solve equation (25) only for values of k in the interval $0 < k < \pi/d$.

In the absence of the periodic corrugations of the perfectly conducting surface, the resulting planar surface does not support a true surface wave, only a surface-skimming

bulk wave, whose dispersion relation is $\omega = c|k|$, the vacuum light line. When the portions of this curve in the second, third, … , Brillouin zones are folded into the first Brillouin zone $-\pi/d < k < \pi/d$, by translations to the left and right by multiples of $2\pi/d$, the result is a zig-zag dispersion curve with a second, third, … branch in addition to the lowest frequency branch. It is the modification of this dispersion curve by the periodic corrugations of the surface that we seek here.

In the nonradiative region of the (k, ω) plane, defined by $|k| > (\omega/c)$, the matrix whose determinant appears in equation (25) is real and symmetric, because of properties of the matrix element S_{jm}, and the fact that $\alpha_0(k_m)$ is pure imaginary with a positive imaginary part for all m. From equation (24) we see that this is required in order that equation (24) describe a surface wave whose amplitude decays exponentially with increasing x_3. The solutions of equation (25) in this region are real and correspond to true surface waves.

For k and ω outside the non-radiative region, the matrix in equation (25) is no longer real and symmetric because some $\alpha_0(k_m)$ become complex with a positive real part, and thus represent components in the sum (24) that radiate into the vacuum. As the surface wave radiates into the vacuum it must decrease in amplitude. To describe this conversion of surface waves into bulk waves in the vacuum we will consider ω to be complex and k to be real. The imaginary part of ω gives the inverse lifetime of the amplitude of the leaky surface wave.

In order to obtain solutions of equation (25) that possess these properties, we have to choose correctly the branch cut that defines the square root in the definition of $\alpha_0(k_n)$. We begin by setting

$$\omega(k) = \omega_{\mathrm{R}}(k) - \mathrm{i}\omega_{\mathrm{I}}(k), \tag{27}$$

where $\omega_{\mathrm{R}}(k)$ and $\omega_{\mathrm{I}}(k)$ are real and positive functions of k. The positivity of $\omega_{\mathrm{I}}(k)$ is needed in order to have a wave whose amplitude decays in time as it propagates. With equations (2) and (27) we have

$$\alpha_0^2(k_n) = \left[\frac{\omega_{\mathrm{R}}^2 - \omega_{\mathrm{I}}^2}{c^2} - \left(k + \frac{2\pi n}{d}\right)^2\right] - \mathrm{i}\frac{2\omega_{\mathrm{R}}\omega_{\mathrm{I}}}{c^2}. \tag{28}$$

We see that $\alpha_0^2(k_n)$ must be in either the third or fourth quadrant. Thus, if we choose the branch cut along the negative real axis, we would always obtain $\alpha_0(k_n)$ in the fourth quadrant, with a positive real part and a negative imaginary part. This means that when $\alpha_0^2(k_n)$ is in the third quadrant, $(\omega_{\mathrm{R}}^2 - \omega_{\mathrm{I}}^2)/c^2 < k_n^2$ i.e. in the nonradiative region, the negative sign of the imaginary part of $\alpha_0(k_n)$ means that the nth term in equation (24) increases exponentially into the vacuum with increasing x_3. This is the opposite of the physical situation we must describe. However, if we take the branch cut along the negative imaginary axis, when $\alpha_0^2(k_n)$ is in the third quadrant $\alpha_0(k_n)$ will be in the second quadrant, with a negative real part and a positive imaginary part. In this case the nth term in equation (24) decreases exponentially with increasing x_3, as is required of a surface wave. Moreover, when $\alpha_0^2(k_n)$ is in the fourth quadrant, $(\omega_{\mathrm{R}}^2 - \omega_{\mathrm{I}}^2)/c^2 > k_n^2$, i.e. in the radiative region, $\alpha_0(k_n)$ is also in the fourth quadrant, with a positive real part and a negative imaginary part. The positive real part of $\alpha_0(k_n)$ corresponds to a wave that is radiating from the surface into the vacuum, as we wish for a radiative or leaky surface wave. The negative imaginary part of $\alpha_0(k_n)$ in this case corresponds to a wave whose amplitude increases exponentially with increasing x_3. This exponential increase of the amplitude of a leaky surface wave with increasing distance from the surface is physically correct. It has been discussed in detail by Lim and Farnell [26], by Ingebrigtsen and Tonning [27], and by Glass and Maradudin [28] in the context of leaky surface acoustic waves, and we refer the reader to these papers for an explanation of this counterintuitive result.

Numerical details: we begin the numerical calculation of the dispersion curve by approximating the infinitely dimensional equation system for $\{A_n\}$ by a finite dimensional system. To this end, we assume $|m| \leqslant M$ and $|n| \leqslant M$ (with M a positive integer) in equation (22), so that the dimension of the resulting linear system becomes $\mathcal{M} = 2M + 1$. The dispersion curve for surface electromagnetic waves that we are interested in is determined by the vanishing of the determinant $D(k, \omega)$ defined in equation (25). However, this quantity, like any determinant, is a highly non-linear and non-continuous function of its parameters. For instance, a slight variation of k and ω may result in orders of magnitude changes in $D(k, \omega)$. Therefore, the function $D(k, \omega)$ is not well suited for being used in a numerical minimization routine. It is well known that a matrix is singular, and hence its determinant vanishes, if and only if one of its eigenvalues vanishes. Hence, we define the function

$$\Lambda(k, \omega) = \min\left\{\left|\lambda_m(k, \omega)\right|\right\}_{m=-M}^{M}, \tag{29}$$

where λ_m denotes one of the eigenvalues of the $\mathcal{M} \times \mathcal{M}$-matrix that has $D(k, \omega)$ as its determinant (see equation (25)). Since $D(k, \omega) = \prod_{m=-M}^{M} \lambda_m(k, \omega)$, it follows that the condition $D(k, \omega) = 0$ is equivalent to $\Lambda(k, \omega) = 0$ which, therefore, represents an alternative definition for the dispersion curve for surface waves. However, we have found the latter definition to be better behaved numerically than the former, and the calculations presented in this work are therefore based on this condition for the existence of surface waves.

To obtain the dispersion curve for surface waves, a mesh of $N + 1$ equally spaced points $k_\ell = \ell\Delta k$, with $\ell = 0, 1, 2, \ldots, N$ and $\Delta k = (\pi/d)/N$, is created in the interval $(0, \pi/d)$ of the k axis, where N is typically 100. For each value k_ℓ, a numerical minimization of the function $\Lambda(k_\ell, \omega)$ is performed with respect to the complex angular frequency $\omega(k) = \omega_{\mathrm{R}}(k) - \mathrm{i}\omega_{\mathrm{I}}(k)$. To this end, we use the Nelder–Mead optimization algorithm [29–31] by considering Λ a function of the two real variables ω_{R} and ω_{I} ($\omega_{\mathrm{R}} \geqslant 0$, $\omega_{\mathrm{I}} \geqslant 0$) but with k_ℓ treated as a known parameter. The minimization starts by assuming a value k_ℓ on the zone boundary of the first Brillouin zone; for odd branches of the

dispersion relation we start at $\ell = 0$ and step forward towards $\ell = N$; for even branches we do the opposite and step downwards from $\ell = N$ towards $\ell = 0$. For each value of k_ℓ an independent numerical minimization of $\Lambda(k_\ell, \omega)$ is performed to identify the complex angular frequency $\omega(k_\ell)$. To make sure that the point indeed is on the dispersion curve for surface waves we recorded both the smallest eigenvalue in modulus of the matrix of equation (25) (i.e. $\Lambda(k_\ell, \omega(k_\ell))$) and its reciprocal condition number. When the calculations were performed in double precision, typical values for these quantities were found to be *at least as small* as 10^{-15} and 10^{-16}, respectively. Only for a small number of points on the dispersion curve did we find values for the reciprocal condition number that were larger than these values; however, for *all* points on the dispersion curve the reciprocal condition number remained several orders of magnitude smaller than one.

In order to follow a given branch of the dispersion curve, some care has to be taken when specifying the initial value for ω used by the minimization routine. For instance, for the first (or fundamental) branch, corresponding to a true surface wave, the minimization starts at $k_0 = 0$ with the initial guess $\omega_{\rm R}(k_0) = \omega_{\rm I}(k_0) = 0$; as ℓ is increased, the initial values used for $\omega_{\rm R}$ and $\omega_{\rm I}$ when performing the minimization at k_ℓ are $\omega_{\rm R}(k_{\ell-1})$ and $\omega_{\rm I}(k_{\ell-1})$, respectively. This means that at step $\ell > 0$, one assumes for the initial value of the frequency the value $\omega(k_{\ell-1})$ that was identified at the previous step $\ell - 1$. In this way the first branch of the dispersion relation is identified, and the approach seemed to work well for all the parameters of the grating that we considered and tested.

We note that for the first branch, it is expected that the imaginary part of the angular frequency is zero, $\omega_{\rm I} = 0$. This we indeed also found in our numerical results, even if the approach used to obtain them made no *a priori* assumption about a zero imaginary part.

For the higher order branches, the initial values for $\omega_{\rm R}(k)$ and $\omega_{\rm I}(k)$ used by the minimization routine were found to depend somewhat more on the parameters defining the grating. However, for the numerical results presented in this work the initial values $\omega_{\rm R} d/(c\pi) = n - 1$ and $\omega_{\rm I} = 0$ were used successfully for the first k-point of the n*th* branch of the dispersion curve located on the left (odd branches) or right (even branches) zone boundary of the first Brillouin zone. For the remaining k_ℓ values ($\ell > 0$) on a higher order branch, we again successfully used $\omega_{\rm R}(k_{\ell-1})$ as the initial value for the frequency in the minimization. In this fashion, the second and third branches of the dispersion curve were identified.

4. Results

To illustrate the preceding results we present results for the dependence of the reflectivity and several other diffraction efficiencies on the angle of incidence θ_0 when several realizations of the perfectly conducting lamellar grating depicted in figure 1 are illuminated by p-polarized light. To help in interpreting the results we note that the value of θ_0 at which the Rayleigh anomalies are expected to occur are obtained from the equation

$$\sin\theta_0^{(m)} = \pm 1 + m\frac{\lambda}{d}, \tag{30}$$

where m is an integer, λ is the wavelength of the incident light, and d is the period of the grating. We note that if a value $\theta_0^{(m)}$ is obtained for some integer value of m when the + sign appears on the right-hand side of this equation, then the value $\theta_0^{(-m)} = -\theta_0^{(m)}$ is obtained for the same magnitude of m but with the opposite sign when the—sign appears on the right-hand side.

The values of θ_0 at which Wood anomalies are predicted to occur are obtained from the equation

$$\frac{\omega}{c}\sin\theta_0 = k_{\rm s}(\omega) + n\frac{2\pi}{d}, \tag{31}$$

where $k_{\rm s}(\omega)$ is the wavenumber of the surface wave of frequency ω and n is an integer. It is convenient to rewrite equation (31) as

$$\sin\theta_0 = \frac{\lambda}{d}\left[\frac{1}{2}\frac{k_{\rm s}(\omega)d}{\pi} + n\right]. \tag{32}$$

The value of $k_{\rm s}(\omega)$ is confined to the interval $0 \leqslant k_{\rm s}(\omega) \leqslant \pi/d$.

The first examples we present to illustrate our results are for a grating defined by the values $a/d = 0.40$ and $h/d = 0.30$. The dispersion curve for the surface electromagnetic waves on this grating, plotted in the reduced zone scheme, is depicted in the left-hand panel of figure 2, where $\omega_{\rm R}(k)$ is plotted as a function of k. It consists of an infinite number of branches, of which we present only the three with the lowest frequencies. We also present in the left-hand panel the vacuum light line folded back into the first Brillouin zone. The right-hand panel presents plots of $\omega_{\rm I}(k)$ as a function of k for each branch of the dispersion curves plotted in the left-hand panel. The magnitude of $\omega_{\rm I}(k)$ gives an indication of the width of the Wood anomaly associated with the excitation of the surface wave of frequency $\omega_{\rm R}(k)$ by incident light of that frequency; the larger $\omega_{\rm I}(k)$, the broader the anomaly.

We present the dependencies of the first several diffraction efficiencies of this grating on the angle of incidence θ_0 in figure 3. The wavelength of the incident light assumed in obtaining these results was $\lambda/d = 0.7350$ [$\omega d/c\pi = 2.7212$]. This corresponds to a point on the third branch of the dispersion curve plotted in figure 2 defined by $k_{\rm s}(\omega)d/\pi = 0.7551$. For these values of the grating and experimental parameters equation (30) predicts that Rayleigh anomalies should occur at $\theta_0 = \pm 15.37^\circ$ and $\pm 28.03^\circ$, while equation (32) predicts that Wood anomalies should occur at $\theta_0 = \pm 16.11^\circ$ and $\pm 27.22^\circ$. The angular positions of the Rayleigh and Wood anomalies are indicated by dash-dotted and dashed lines, respectively, in figure 3 and subsequent figures. In the results presented in figure 3 the Rayleigh and Wood anomalies appear at the angles of incidence predicted for them by equations (30) and (32), respectively. In the case of $e_0(\theta_0)$ the Rayleigh anomaly at $\theta_0 = \pm 15.37^\circ$ is a weak dip, while the one at $\theta_0 = \pm 28.03^\circ$ is a vertical slope. Both

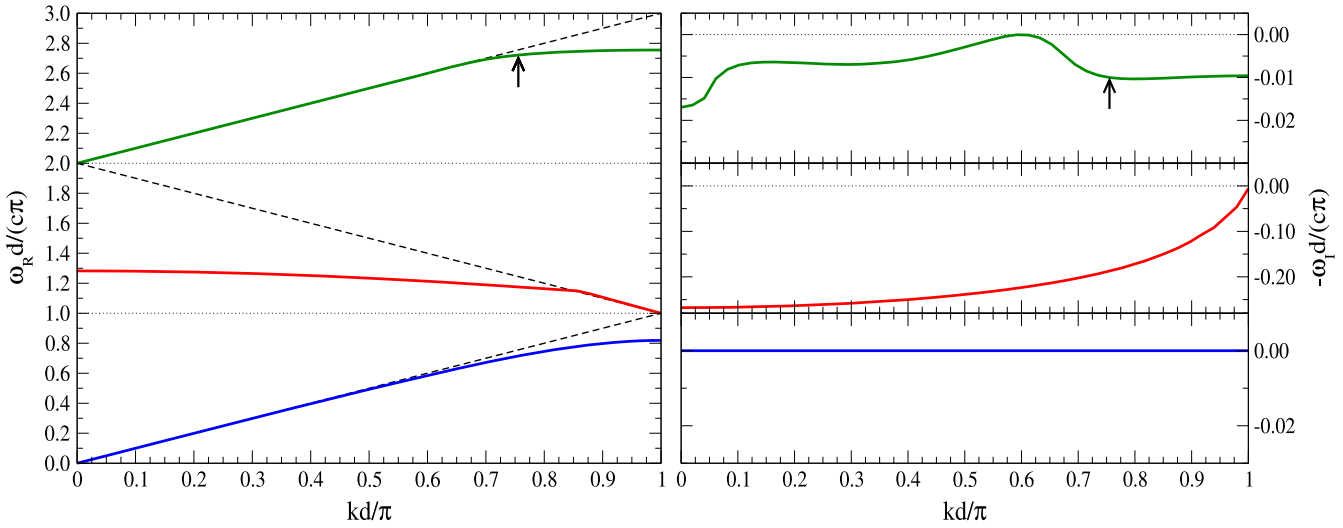

Figure 2. The dispersion curves for the surface electromagnetic waves supported by a lamellar perfectly conducting grating defined by $a/d = 0.40$ and $h/d = 0.30$. Both the real, $\omega_{\rm R}(k)$, and imaginary, $-\omega_{\rm I}(k)$, parts of the frequency $[\omega(k) = \omega_{\rm R}(k) - {\rm i}\omega_{\rm I}(k)]$ of these waves are presented in the reduced zone scheme. The first branch of the dispersion (blue line) is located in the nonradiative region of the (k, ω)-plane, and it corresponds to a *true* surface wave, the imaginary part of whose frequency vanishes identically. The second and third branches of the dispersion curve (red and green lines, respectively) are both located in the radiative region ($|k| < \omega/c$); they correspond to *leaky* surface waves, whose frequencies have negative imaginary parts. The dashed (black) lines denote the vacuum light line in the reduced zone scheme. The arrows correspond to the wavelength $\lambda/d = 0.7350$ $[\omega d/c\pi = 2.7212]$ that will be used to calculate diffraction efficiencies in figure 3. The numerical calculations were done for $M = 10$, but increasing this value, did not affect the final result.

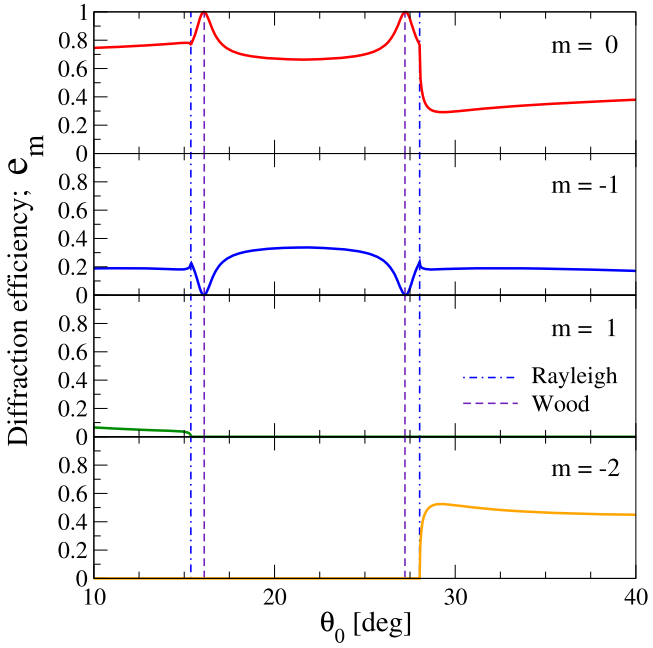

Figure 3. The diffraction efficiencies $e_m(\theta_0)$, equation (19), as functions of the angle of incidence for a lamellar grating defined by $a/d = 0.40$ and $h/d = 0.30$. The angular positions of the Rayleigh and Wood anomalies, determined by equations (30) and (32), respectively, are indicated by vertical dashed–dotted and dashed lines, respectively. Only diffracted orders m for which $e_m(\theta_0) \neq 0$ in the range of θ_0 considered are presented. The wavelength of the incident light assumed in obtaining these results was $\lambda/d = 0.7350$. The point on the dispersion curve for this grating corresponding to this wavelength is indicated by arrows in figure 2. The numerical calculations were done for $M = 10$.

the Wood anomalies are peaks in this case. In the results presented for $e_{-1}(\theta_0)$, the Rayleigh anomalies are small sharp peaks, while the Wood anomalies are now dips. In the results for $e_1(\theta_0)$ and $e_{-2}(\theta_0)$ no Wood anomalies are present, but the Rayleigh anomalies manifest themselves through the disappearance of a diffracted order and the appearance of a new one, respectively, as θ_0 is increased.

In the numerical calculations that produced the results presented in figures 2 and 3, we assumed $M = 10$ since increasing it further, did not result in any detectable changes in the results obtained, at least not for the grating parameters assumed. In these calculations, the energy conservation condition, equation (20), was checked explicitly and, for all angles of incidence considered, found to deviate from unity by an amount no larger than 10^{-14} in magnitude when the calculations were performed in double precision. Moreover, in all the subsequent calculation results presented in this work we also assumed $M = 10$, and the same satisfactory fulfillment of the energy conservation condition was found for them.

In figure 4 we present plots of $\omega_{\rm R}(k)$ and $\omega_{\rm I}(k)$ as functions of k for surface electromagnetic waves on a grating defined by $a/d = 0.45$ and $h/d = 0.20$. The first several diffraction efficiencies of this grating are plotted as functions of θ_0 in figure 5. The wavelength of the incident light assumed in obtaining this figure was $\lambda/d = 0.7518$ $[\omega d/c\pi = 2.660]$. This corresponds to a point on the third branch of the dispersion curve plotted in figure 4 defined by $k_{\rm s}(\omega)d/\pi = 0.7551$. For these values of the parameters Rayleigh anomalies are predicted by equation (30) to occur at

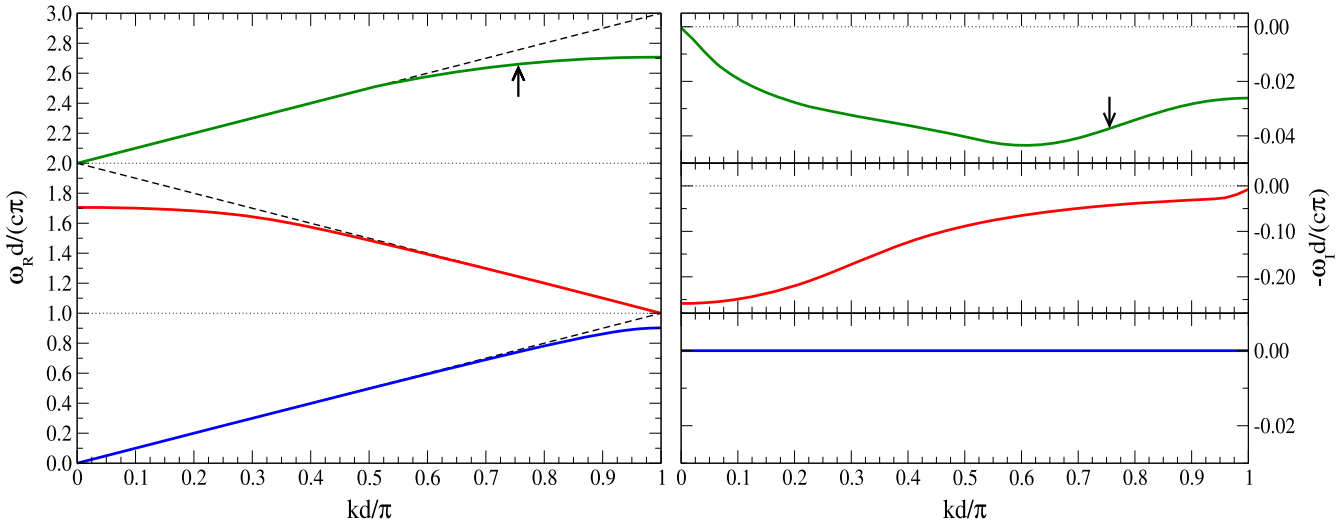

Figure 4. The same as figure 2, but now for a grating defined by $a/d = 0.45$ and $h/d = 0.20$. The arrows correspond to a wavelength $\lambda/d = 0.7518$ [$\omega d/c\pi = 2.660$], which will be used in calculating the diffraction efficiencies in figure 5.

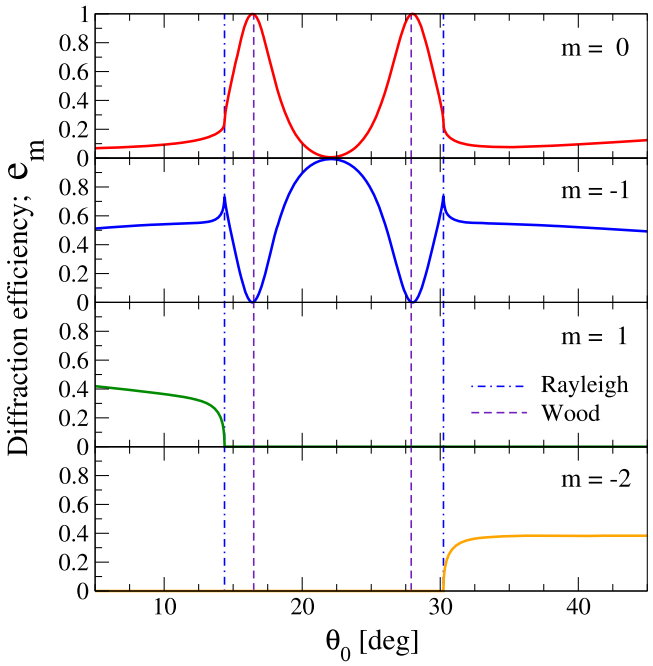

Figure 5. The same as figure 3, but now for a grating defined by $a/d = 0.45$ and $h/d = 0.20$. The wavelength of the incident light is $\lambda/d = 0.7518$ (indicated by the arrows in figure 4).

$\theta_0 = \pm 14.37°$ and $\pm 30.23°$, while Wood anomalies are predicted by equation (32) to occur at $\pm 16.49°$ and $\pm 27.90°$. Again, the Rayleigh and Wood anomalies are found to occur at the predicted angular positions. In the case of $e_0(\theta_0)$ the Rayleigh anomalies have the form of vertical slopes at their predicted angular positions, while the Wood anomalies are peaks at their predicted angular positions. The Rayleigh anomalies manifest themselves as sharp peaks in the case of $e_{-1}(\theta_0)$, while theWood anomalies are broad dips at $\theta_0 = \pm 16.49°$ and $\pm 27.90°$. In the case of $e_1(\theta_0)$ and $e_{-2}(\theta_0)$ no Wood anomalies are predicted, and the Rayleigh anomalies correspond to the disappearance and appearance of diffracted orders, respectively.

For our third example we consider a grating defined by $a/d = 0.60$ and $h/d = 0.20$. In figure 6 we present the dependencies of $\omega_R(k)$ and $\omega_I(k)$ on k. We assume that this grating is illuminated by light whose wavelength is $\lambda/d = 0.8867$ [$\omega d/c\pi = 2.2554$]. This corresponds to a point on the third branch of the dispersion curve plotted in figure 6 defined by $k_s(\omega)d/\pi = 0.4490$. From equations (30) to (32) we find that Rayleigh anomalies are predicted to occur at $\theta_0 = \pm 6.50°$ and $\pm 50.67°$, while Wood anomalies are predicted to occur at $\theta_0 = \pm 16.11°$ and $\pm 27.22°$. We see from figure 7 that these anomalies occur at the predicted angles of incidence.

For our final example we display the coalescence of two Wood anomalies as the grooves of a grating are made shallower for a fixed value of the width of the grooves [figure 8]. The grating chosen for this study is defined by $a/d = 0.60$ and four values of h/d namely 0.20, 0.19, 0.17, and 0.15. The calculation of the angular dependencies of the diffraction efficiencies $e_0(\theta_0)$ and $e_{-1}(\theta_0)$ were carried for each grating for a value $k_s(\omega)d/\pi = 0.7551$. Consequently the values of λ/d varied from grating to grating. For a value of $h/d = 0.20$, we see two Wood anomalies in $e_0(\theta_0)$ at the predicted values $\theta_0 = \pm 18.55°$ and $\pm 31.63°$. They are broad, as is to be expected from the magnitude of the imaginary part of the frequency on the third branch of the dispersion curve at the wavenumber $k_s(\omega)d/\pi = 0.7551$ presented in figure 6. The dips centered at these angles in $e_{-1}(\theta_0)$ are also broad, for the same reason. The Rayleigh anomalies occurring at $\theta_0 = 9.05°$ and $43.25°$ are dips in $e_0(\theta_0)$ and peaks in $e_{-1}(\theta_0)$. As the value of h/d is decreased the Wood and Rayleigh anomalies move closer together, until at $h/d = 0.15$ the Wood anomalies overlap sufficiently to produce a single peak in $e_0(\theta_0)$ and a single dip in $e_{-1}(\theta_0)$. The Rayleigh anomalies do not come sufficiently close to overlap for the values of the grating parameters assumed in preparing this figure. The

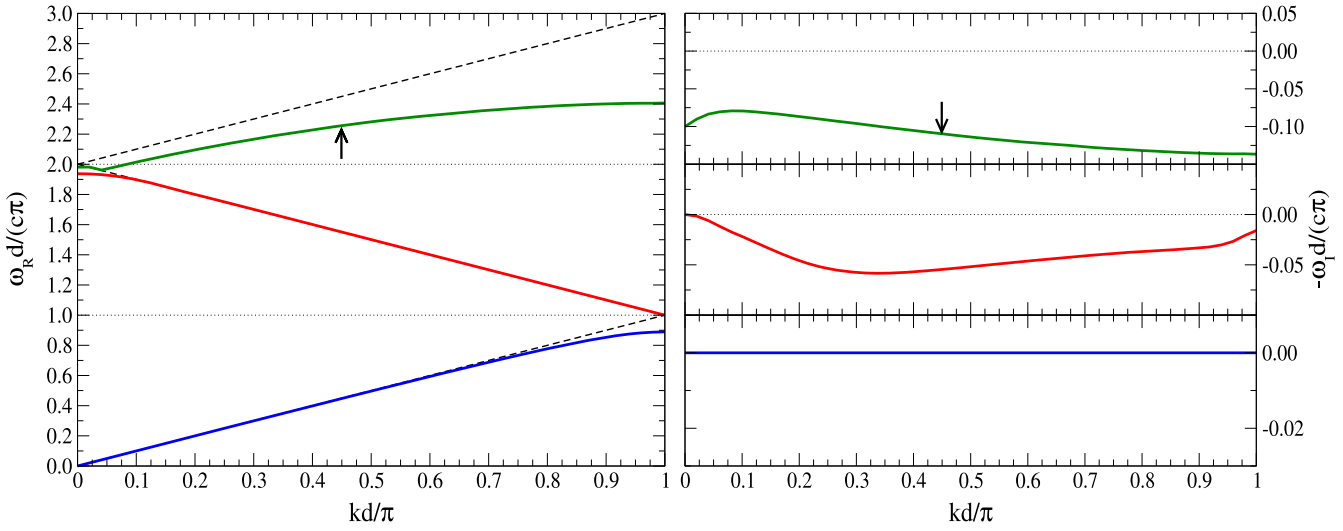

Figure 6. The same as figure 2, but now for a grating defined by $a/d = 0.60$ and $h/d = 0.20$. The arrows correspond to the wavelength $\lambda/d = 0.8867$ [$\omega d/c\pi = 2.2554$], which will be used in calculating the diffraction efficiencies presented in figure 7.

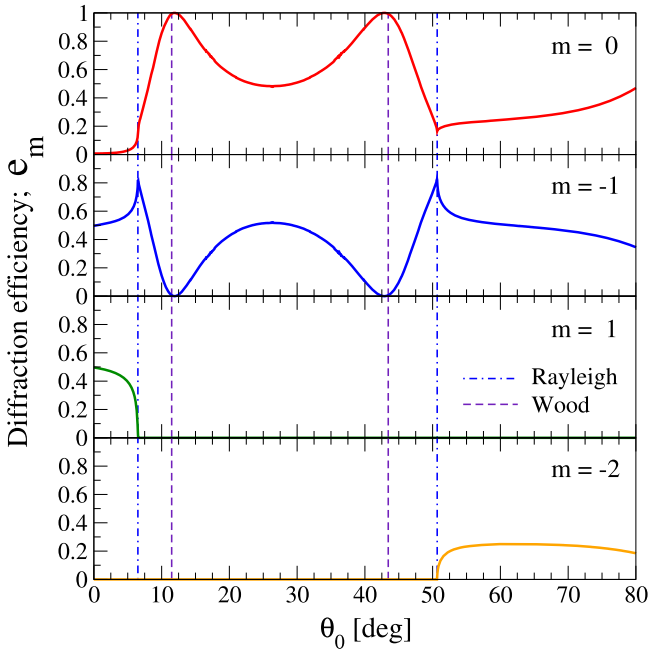

Figure 7. The same as figure 3, but now for a grating defined by $a/d = 0.60$ and $h/d = 0.20$. The wavelength of the incident light is $\lambda/d = 0.8867$ (indicated by the arrows in figure 6).

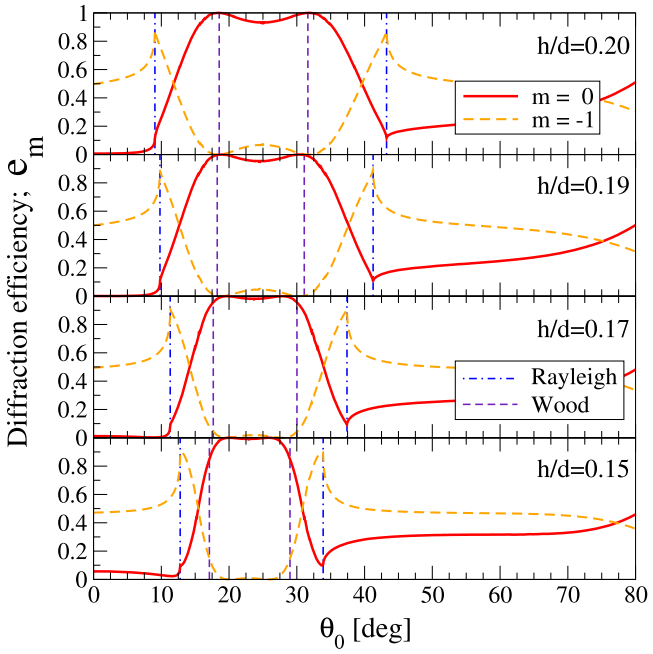

Figure 8. The diffraction efficiencies, $e_0(\theta_0)$ and $e_{-1}(\theta_0)$, as functions of the angle of incidence θ_0 for a grating defined by $a/d = 0.60$, and several values of h/d, as indicated on the figure. In obtaining these curves the value $kd/\pi = 0.7551$ was assumed.

forms of both the Wood and Rayleigh anomalies remain unchanged as h/d is decreased.

5. Conclusions

We have shown that when a perfectly conducting lamellar grating is illuminated from vacuum by p-polarized light whose plane of incidence is perpendicular to the grooves of the grating, the angular dependencies of the diffraction efficiencies display Rayleigh and Wood anomalies. The former anomalies occur at the angles predicted by Rayleigh [4]. The positions of the Wood anomalies occur at the angles associated with the excitation of the surface electromagnetic waves supported by the periodically corrugated surface, as predicted by Fano [7] in his study of these anomalies in diffraction from a metallic grating.

By calculating the dispersion curves of the surface electromagnetic waves supported by the grating in both the nonradiative and radiative regions of the frequency-wave number plane, we have been able to relate the angles of incidence at which the Wood anomalies occur at a given wavelength of the incident light to the wavenumber of the surface wave corresponding to that wavelength, something

not done in earlier studies of diffraction from perfectly conducting gratings.

In a sense our result extends the work of Fano in showing that it is the existence of a surface wave on a periodically corrugated surface, of whatever nature, not only a surface plasmon polariton, as in the case considered by Fano, that gives rise to the Wood anomalies. Thus, these anomalies can also be expected to occur in the diffraction of volume waves from other types of periodically corrugated impenetrable surfaces that support surface waves. As an example of this, because the periodically corrugated surface of an elastic medium in contact with vacuum, which plays the role of the impenetrable medium, supports surface acoustic waves of sagittal and shear horizontal polarizations [32], we can expect the occurrence of Wood (and Rayleigh) anomalies in the angular dependencies of the reflectivity of bulk acoustic waves of sagittal and shear horizontal polarizations incident on such a surface. This effect should be studied theoretically and experimentally.

Acknowledgments

The research of IS was supported in part by The Research Council of Norway Contract No. 216699. The work of RMF was partially supported by the National Oceanic and Atmospheric Administration, Educational Partnership Program, US Department of Commerce, under Agreement No. NA11SEC4810003.

References

[1] Wood R W 1902 On a remarkable case of uneven distribution of light in a diffraction grating *Phil. Mag.* **4** 396–402
[2] Wood R W 1902 On a remarkable case of uneven distribution of light in a diffraction grating spectrum *Proc. Phys. Soc.* **18** 269–75
[3] Rayleigh L 1907 On the dynamical theory of gratings *Proc. R. Soc.* A **79** 399–416
[4] Rayleigh Lord 1907 Note on the remarkable case of diffraction spectra described by Prof. Wood *Phil. Mag.* **14** 60–5
[5] Wood R W 1912 Diffraction gratings with controlled groove form and abnormal distribution of intensity *Phil. Mag.* **23** 310–7
[6] Palmer C H Jr 1952 Parallel diffraction grating anomalies *J. Opt. Soc. Am.* **43** 269–73
[7] Fano U 1941 The theory of anomalous diffraction gratings and of quasi-stationary waves on metallic surfaces Sommerfeld's waves *J. Opt. Soc. Am.* **3** 213–22
[8] Nevière M 1980 The homogeneous problem *Electromagnetic Theory of Gratings* ed R Petit (Berlin: Springer) pp 123–157
[9] Ulrich R and Tacke M 1973 Submillimeter waveguiding on periodic metal structure *Appl. Phys. Lett.* **22** 251–3
[10] Maystre D 2012 Theory of Wood's anomalies *Plasmonics* ed S Enoch and N Bonod (Berlin: Springer) pp 39–83
[11] Petit R 1965 Etude numérique de la diffraction par un réseau *C. R. Acad. Sci., Paris* **260** 4454–7
[12] Petit R 1966 Contribution á l'étude de la diffraction par un réseau metallique *Rev. Opt.* **45** 249–76
[13] Wirgin A 1964 Considérations théoriques sur la diffraction par réflexion sur des surfaces quasiment planes applications á la diffraction par des réseaux *C. R. Acad. Sci., Paris* **259** 1486–8
[14] Pavageau J and Bousquet J 1970 Diffraction par un réseau conducteur nouvelle méthode de réseau conducteur nouvelle méthode de résolution *Opt. Acta* **17** 469–78
[15] McPhedran R C and Waterworth M D 1973 Properties of diffraction grating anomalies *Opt. Acta* **20** 533–47
[16] Hessel A and Oliner A A 1965 A new theory of Wood's anomalies on optical gratings *Appl. Opt.* **4** 1275–97
[17] Hutley M C 1973 An experimental study of the anomalies of sinusoidal diffraction gratings *Opt. Acta* **20** 607–24
[18] Hutley M C and Bird V M 1973 A detailed experimental study of the anomalies of a sinusoidal diffraction grating *Opt. Acta* **20** 771–82
[19] Mills D L and Maradudin A A 1989 Surface corrugation and surface polariton binding in the infrared frequency range *Phys. Rev.* B **39** 1569–74
[20] Pendry J B, Martín-Moreno L and García-Vidal F J 2004 Mimicking surface plasmons with structured surfaces *Science* **305** 847–8
[21] López-Rios T, Mendoza D, García-Vidal F J, Sánchez-Dehesa J and Pannetier B 1998 Surface shape resonances in lamellar metallic gratings *Phys. Rev. Lett.* **81** 665–8
[22] García-Vidal F J, Sanchez-Dehesa J, Dechelette A, Bustarret E, López-Rios T, Fournier T and Pannetier B 1999 Localized surface plasmons in lamellar metallic gratings *J. Lightwave Technol.* **17** 2191–5
[23] Maystre D and Petit R 1972 Diffraction par un reseau lamellaire infiniment conducteur *Opt. Commun.* **5** 90–3
[24] Bloch F 1928 Uber die quantenmechanik der electronen in kristallgittern *Z. Phys.* **52** 555–600
[25] Simonsen I 2010 Optics of surface disordered systems: a random walk through rough surface scattering phenomena *Eur. Phys. J.—Spec. Top.* **181** 1–03
[26] Lim T C and Farnell G W 1969 Character of pseudo surface waves on anisotropic crystals *J. Acoust. Soc. Am.* **45** 845–51
[27] Ingebrigtsen K A and Tonning A 1969 Elastic surface waves in crystals *Phys. Rev.* **184** 942–51
[28] Glass N E and Maradudin A A 1983 Leaky surface-elastic waves on both flat and strongly corrugated surfaces for isotropic, non dissipative media *J. Appl. Phys.* **54** 796–805
[29] Nelder J A and Mead R 1965 A simplex method for function minimization *Comput. J.* **7** 308–13
[30] O'Neill R 1971 Algorithm AS47—function minimization using a simplex procedure *Appl. Stat.* **20** 338–45
[31] Lagarias J C, Reeds J A, Wright M H and Wright P E 1998 Convergence properties of the Nelder–Mead simplex method in low dimensions *SIAM J. Optim.* **9** 112–47
[32] Maradudin A A and Zierau W 1994 Surface acoustic waves of sagittal and shear horizontal polarizations on large-amplitude gratings *Geophys. J. Int.* **118** 325–32